Research Square

Preprints are preliminary reports that have not undergone peer review.
They should not be considered conclusive, used to inform clinical practice,
or referenced by the media as validated information.

Stability Analysis of Multi-Serial-Link Mechanism Driven by Antagonistic Multiarticular Artificial Muscles

Yuta Ishikawa (ishikawa.y.as@m.titech.ac.jp)
Tokyo Institute of Technology: Tokyo Kogyo Daigaku https://orcid.org/0000-0001-7294-2222
Hiroyuki Nabae
Tokyo Institute of Technology: Tokyo Kogyo Daigaku
Gen Endo
Tokyo Institute of Technology: Tokyo Kogyo Daigaku
Koichi Suzumori
Tokyo Institute of Technology: Tokyo Kogyo Daigaku

Research Article

Keywords: artificial muscle, bioinspired robot, multi-serial-link mechanism, antagonistic-muscle-driven system

Posted Date: October 25th, 2021

DOI: https://doi.org/10.21203/rs.3.rs-968693/v1

License: This work is licensed under a Creative Commons Attribution 4.0 International License.
Read Full License

Stability analysis of multi-serial-link mechanism driven by antagonistic multiarticular artificial muscles

Yuta Ishikawa[1*], Hiroyuki Nabae[1], Gen Endo[1] and Koichi Suzumori[1]

*Corresponding author: ishikawa.y.as@m.titech.ac.jp

[1] Department of Mechanical Engineering, Tokyo Institute of Technology, 2-12-1 Ookayama, Meguro-ku, Tokyo 152-8550, Japan.

Abstract

Artificial multi-joint musculoskeletal systems consisting of serially connected links driven by monoarticular and multiarticular muscles, which are often inspired by vertebrates, enable robots to elicit dynamic, elegant, and flexible movements. However, serial links driven by multiarticular muscles can cause unstable motion (e.g., buckling). The stability of musculoskeletal mechanisms driven by antagonistic multi-joint muscles depends on the muscle configuration, origin/insertion of muscles, spring constants of muscles, contracting force of muscles, and other factors. We analyze the stability of a multi-serial-link mechanism driven by antagonistic multi-joint muscles aiming to prevent buckling and other undesired motions. First, we theoretically derive the potential energy of the system and the stable condition at the target point. Then, we validate the method through dynamic simulations and experiments. We confirm that we can construct a stable multiarticulate musculoskeletal system using the proposed formulation and conditions.

Keywords: artificial muscle, bioinspired robot, multi-serial-link mechanism, antagonistic-muscle-driven system

Introduction

Vertebrates, including humans, have multiarticulate musculoskeletal systems that allow to voluntarily exert large forces and perform flexible movements with adaptability to the environment. A musculoskeletal system has two types of muscles: multiarticular muscles that span two or more joints and act on the joints simultaneously and monoarticular muscles that act on a single joint. Multiarticular muscles are thought to enable large movements involving large parts of the musculoskeletal system, while monoarticular muscles are mainly used for small movements and joint support.

We have developed an artificial multiarticulate musculoskeletal robot that mimics the structure of necks of giraffes and humans [1, 2]. We have observed that the robot curves like a bow or buckles in zigzag when multiarticular muscles, such as the longus colli, are driven without sufficient stiffness at each joint (Figs. 1 and 2). Figure 2 shows a diagram of buckling in the developed system. In an animal, monoarticular muscles, intervertebral discs, and constructions that increase joint stiffness prevent such deformation. Although musculoskeletal robots can achieve high power and flexibility, deformation remains a major challenge. Therefore, we aimed to characterize the buckling problem for a multiarticulate musculoskeletal system and use the resulting formulation in the design of musculoskeletal robots.

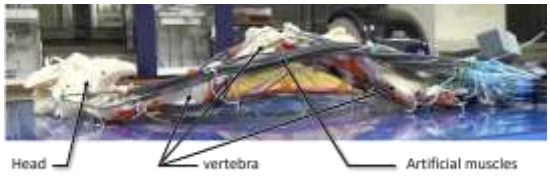

Fig. 1 Musculoskeletal robot of giraffe neck developed in-house and showing buckling

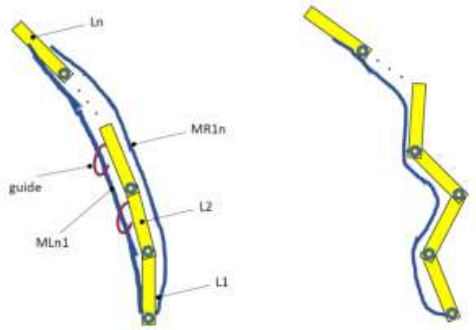

Fig. 2 Zigzag buckling of multi-serial-link mechanism driven by antagonistic multiarticular muscles without sufficient support from monoarticular muscles

Various types of robots driven by multiarticular muscles mimicking upper and lower limbs , vertebrae, and other anatomical structures have been proposed. The endpoint stiffness control of robots mimicking human upper limbs has been studied for a three-bar serial-link model driven by monoarticular and biarticular muscles [3, 4]. In addition, a stable muscle arrangement has been studied using similar models [5]. However, as only two joints and biarticular muscles have been considered, no zigzag buckling can occur. Moreover, although the stability from the viewpoint of potential energy has been discussed [5], the tensile force of muscles has been assumed to be constant relative to length, being unsuitable to describe pneumatic artificial muscles, whose tensile force and stiffness vary according to the length and driving force, respectively.

For multiarticulate musculoskeletal lower-limb robots, control of both the reaction force from the ground and the jumping force has been conducted considering muscle elasticity [6–8]. Similar to upper-limb robots, two joints with biarticular muscles have been considered. The stiffness of the biarticular muscle and muscle model of the lower limb as a passive spring were studied in [6]. In [7], antagonistic

57 muscles spanned different joints, and in [8], a model with antagonistic biarticular muscles that spanned
58 the same joints was derived. However, none of these studies have addressed instability in the
59 musculoskeletal system.

60 Studies on multiarticulate musculoskeletal robots mimicking the upper and lower limbs have dealt
61 with systems driven by multiarticular muscles spanning three or more joints. However, the instability
62 conditions that we address have been neglected. Multiarticulate musculoskeletal robots consisting of
63 three or more joints and multiarticular muscles spanning the joints have been inspired by the spine of
64 animals such as humans [9, 10], lancelets [11], and snakes [12, 13]. The robots introduced in [9, 10]
65 consisted of silicone rubber to support each joint, but their instability conditions were neglected. In [11],
66 lancelet swimming was studied using a nine-joint musculoskeletal system with seven pairs of tri-
67 articular muscles, which were arranged antagonistically. However, each antagonistic pair was driven
68 by one motor, preventing the analysis of simultaneous contraction of antagonistic muscles and system
69 buckling. In [12], snake locomotion was simulated, and the efficiency of multiarticular muscles was
70 studied by changing the number of joints spanned by monoarticular up to tri-articular muscles. In [13],
71 the superiority of multiarticular muscles over monoarticular muscles was verified with respect to force
72 per cross-sectional area and energy efficiency. However, instability was not addressed.

73 In [14], the stability of multi-joint tendon-driven robots was studied in general considering the elastic
74 energy of the tendons, and the minimum length that the tendons must be stretched was theoretically
75 derived. However, in the corresponding wire rope–pulley system, the moment arm around each joint

exerted by tension of each wire was assumed to be constant. Consequently, the analysis of this system cannot be applied to musculoskeletal systems, in which the moment arm changes nonlinearly with respect to the joint angles.

Although various studies on multiarticulate musculoskeletal systems are available, few existing multiarticular muscles span three or more joints, and buckling that may occur when activating multiarticular muscles has been neglected. Moreover, the posture stability when antagonistic multiarticular muscles contract simultaneously and when the muscle stiffness changes with the driving force has not been studied. Therefore, the adequate force and stiffness of monoarticular and multiarticular muscles for stable operation of a musculoskeletal system remain to be determined.

Considering that the stiffness of most animal muscles and artificial muscles physically changes with the driving force, we aimed to clarify the required parameters of monoarticular and multiarticular muscles to avoid buckling during multiarticular muscle activation. Specifically, we analyzed the static stability of a multiarticulate musculoskeletal system using the potential energy of the system using a multi-serial-link mechanism and modeling the artificial muscles as spring elements. In addition, we considered static stability as the system convergence to a target angle and buckling instability if the system buckles in zigzag or bends uniformly like a bow. In addition to the model analysis, we verified the stability formulation through both dynamic simulations implemented in MathWorks MATLAB and experiments using McKibben artificial muscles.

Methods

Modeling and stability analysis

Our model of musculoskeletal system is the planar multi-serial-link mechanism antagonistically driven by artificial muscles shown in Fig. 3a. Figure 3b illustrates the fixed position of the multiarticular muscles spanning from joint p to joint q. Figure 3 shows the m-th pair of antagonistic muscles attached to vertical fixtures at distance a_m from the axis along each link and at distances $e_{0,m}$ and $e_{1,m}$ from each joint along each link. Thus, $e_{0,m}$ and $e_{1,m}$ represent the distance of a joint with a number and that of a joint with the subsequent number, respectively. In addition, the stiffness of the left and right sides of the m-th pair of antagonistic muscles, the link lengths, and the joint angles are denoted as $K_{L,m}$, $K_{R,m}$, $l_0 \ldots l_N$, and $\theta_1 \ldots \theta_N$, respectively. Both sides of each antagonistic muscle are driven with the same contraction force, as detailed below.

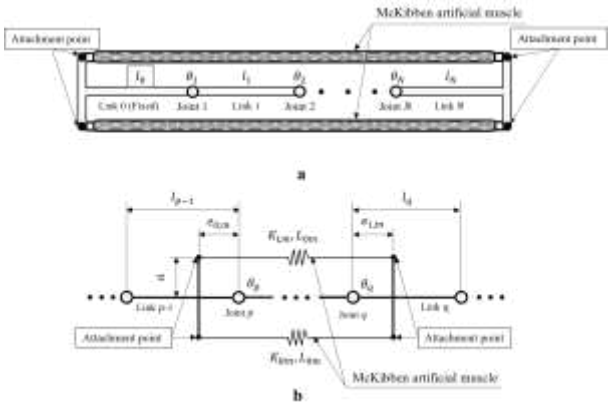

Fig. 3 Model of multi-serial-link mechanism driven by McKibben artificial muscles. **a** N-serial-link mechanism and **b** arrangement of antagonistic multi-joint muscles represented as springs. The stiffnesses of the left and right sides and the natural length of the m-th artificial muscle are denoted as $K_{L,m}$, $K_{R,m}$, and $L_{0,m}$, respectively

McKibben artificial muscle

We used McKibben pneumatic artificial muscles in this study. For the experiments, we used McKibben muscles with a diameter of 2 mm. This type of artificial muscle mainly consists of an inner rubber tube to which air pressure is applied, and an outer sleeve of a woven fiber intersects at a certain angle. The sleeve contracts through expansion in the radial direction of the inner tube.

Among the various formulations, the simplest equation to describe the McKibben muscle operation has been proposed by Schulte [15]:

$$F = \frac{\pi D^2}{4\sin^2\theta_0} P\{3(1-\varepsilon)^2\cos^2\theta_0 - 1\} \tag{1}$$

where $F, D, P, \theta_0,$ and ε are the contraction force, diameter of the inner tube, air pressure applied to the tube, woven angle of the sleeve, and contraction ratio of the artificial muscle, respectively. Equation (1) is based on the virtual work principle. The work done by both the compressed air applied to the rubber tube and the artificial muscle are assumed to be the equal. Thus, the corresponding geometric calculation neglects the elasticity of the rubber tube and sleeve strands. The maximum contraction force, which occurs when the contraction rate is 0, seems to agree with experimental data, but the maximum contraction ratio may be inconsistent.

In the next section, we approximate the McKibben artificial muscle model as a spring, whose stiffness K and natural length s_0 are given by Eq. (2). The maximum contraction force, F_{Max}, is derived from Eq. (1), and the maximum contraction ratio, $\varepsilon_{\mathrm{Max}}$, can be obtained experimentally.

$$K = \frac{F_{\mathrm{Max}}}{\varepsilon_{\mathrm{Max}} S}, \qquad s_0 = S(1-\varepsilon_{\mathrm{Max}}) \tag{2}$$

Note that S represents the default length of the muscle, and muscle stiffness K varies with driving pressure P.

Potential energy of multi-serial-link mechanism driven by antagonistic artificial muscles

We also consider the stability of the multiarticulate musculoskeletal system driven by antagonistic muscles. We focus on a straight posture, which is common for the spine. For the system to be stable, the potential energy of the entire system, U, must reach a local minimum at the target angles. Therefore, considering an *N*-joint serial-link mechanism, a sufficient condition for stability is given by the entire potential energy, $U(\boldsymbol{\theta})$ ($\boldsymbol{\theta} \in \boldsymbol{R}^N$), satisfying the following condition:

$$\frac{\partial U}{\partial \theta_i} = 0 \quad \text{for } \forall i \in [1, N] \tag{3}$$

$$\boldsymbol{x}^{\boldsymbol{T}}\boldsymbol{H}\boldsymbol{x} > 0 \quad \forall \boldsymbol{x} \in \boldsymbol{R}^N \tag{4}$$

where $\boldsymbol{H} \in \boldsymbol{R}^{\boldsymbol{N}\times\boldsymbol{N}}$ is the Hessian matrix describing the second-order partial derivative of U. Specifically, the element at row *i* and column *j* of matrix $\boldsymbol{H}$ is given by

$$H_{ij} = \frac{\partial^2 U}{\partial \theta_i \partial \theta_j} \quad (\ 1 \le i \le N, 1 \le j \le N \ )$$

Equation (4) is equivalent to the following equation:

$$\det(\boldsymbol{A}_k) > 0 \quad \forall k \in [1, N] \tag{5}$$

$$\boldsymbol{A}_k \equiv \begin{bmatrix} H_{11} & \cdots & H_{1k} \\ \vdots & \ddots & \vdots \\ H_{k1} & \cdots & H_{kk} \end{bmatrix}$$

The potential energy of the entire system, U, can be expressed as the sum of the potential energy

produced by the antagonistic muscles:

$$U = \sum_{m}^{M} \left\{ \frac{K_{L,m}}{2} \left(\left| \boldsymbol{s_{L,m}} \right| - s_{0,m} \right)^2 + \frac{K_{R,m}}{2} \left(\left| \boldsymbol{s_{R,m}} \right| - s_{0,m} \right)^2 \right\} \tag{6}$$

where M is the number of pairs of antagonistic muscles, $\boldsymbol{s_{L,m}}$ and $\boldsymbol{s_{R,m}}$ are the endpoint vectors of the left and right sides of antagonistic muscle m, respectively, and $|\boldsymbol{s}|$ is the norm of vector $\boldsymbol{s}$. We set the natural length of both muscle sides to $s_{0,m}$. As shown in Fig. 3b, the endpoints of the multiarticular muscles that span from joint p to joint q have distances $e_{0,m}$ and $e_{1,m}$ from each joint. As the muscle endpoints are attached to the next links, $e_{0,m}$ and $e_{1,m}$ must satisfy the following constraints:

$$0 \le e_{0,m} \le l_{p-1}, \qquad 0 \le e_{1,m} \le l_q$$

By using the angles of the mechanism, $\boldsymbol{s_{L,m}}$ and $\boldsymbol{s_{R,m}}$ can be described as follows:

$$\boldsymbol{s_{L,m}} = \begin{pmatrix} e_{0,m} + \sum_{n=p}^{q-1} l_n \cos\phi_n + e_{1,m} \cos\phi_q + a_m \sin\phi_q \\ a_m + \sum_{n}^{q-1} l_n \sin\phi_n + e_{1,m} \sin\phi_q - a_m \cos\phi_q \end{pmatrix}$$

$$\boldsymbol{s_{R,m}} = \begin{pmatrix} e_{0,m} + \sum_{n=p}^{q-1} l_n \cos\phi_n + e_{1,m} \cos\phi_q - a_m \sin\phi_q \\ -a_m + \sum_{n}^{q-1} l_n \sin\phi_n + e_{1,m} \cos\phi_q + a_m \cos\phi_q \end{pmatrix}$$

where $\phi_n = \sum_{k=p}^{n} \theta_k$. The only difference between $\boldsymbol{s_{L,m}}$ and $\boldsymbol{s_{R,m}}$ is the change in the positive and negative signs of a_m given the symmetry of the antagonistic muscles.

For antagonistic muscle m, the first- and second-order partial derivatives of its potential energy U_m

are respectively given by

$$\frac{\partial U_m}{\partial \theta_i} = K_{L,m}\left(\left|\boldsymbol{s}_{L,m}\right| - s_{0,m}\right)\frac{\partial \left|\boldsymbol{s}_{L,m}\right|}{\partial \theta_i} + K_{R,m}\left(\left|\boldsymbol{s}_{R,m}\right| - s_{0,m}\right)\frac{\partial \left|\boldsymbol{s}_{R,m}\right|}{\partial \theta_i} \tag{7}$$

$$\begin{aligned}\frac{\partial^2 U_m}{\partial \theta_i \partial \theta_j}\left(= H_{m,ij}\right) &= K_{L,m}\frac{\partial \left|\boldsymbol{s}_{L,m}\right|}{\partial \theta_i}\frac{\partial \left|\boldsymbol{s}_{L,m}\right|}{\partial \theta_j} + K_{L,m}\left(\left|\boldsymbol{s}_{L,m}\right| - s_{0,m}\right)\frac{\partial^2 \left|\boldsymbol{s}_{L,m}\right|}{\partial \theta_i \partial \theta_j} \\ &+ K_{R,m}\frac{\partial \left|\boldsymbol{s}_{R,m}\right|}{\partial \theta_i}\frac{\partial \left|\boldsymbol{s}_{R,m}\right|}{\partial \theta_j} + K_{R,m}\left(\left|\boldsymbol{s}_{R,m}\right| - s_{0,m}\right)\frac{\partial^2 \left|\boldsymbol{s}_{R,m}\right|}{\partial \theta_i \partial \theta_j}\end{aligned} \tag{8}$$

where U_m is assumed to be a continuous and second-order differentiable function in $\boldsymbol{R}^N$, and the order of differentiation can be ignored.

As the target angles are set to $\boldsymbol{\theta} = \vec{0} \in \boldsymbol{R}^N$, we have

$$\left|\boldsymbol{s}_{L,m}\right| = e_{0,m} + \sum_{n}^{p} l_n + e_{1,m} \tag{9}$$

$$\frac{\partial \left|\boldsymbol{s}_{L,m}\right|}{\partial \theta_i} = \frac{a_m\left(e_{0,m} + \sum_{n=p}^{q-1} l_n + e_{1,m}\right)}{e_{0,m} + \sum_{n=p}^{q-1} l_n + e_{1,m}} = a_m \tag{10}$$

$$\frac{\partial^2 \left|\boldsymbol{s}_{L,m}\right|}{\partial \theta_i \partial \theta_j} = \frac{-\left(e_{0,m} + \sum_{n=p}^{i-1} l_n\right)\left(\sum_{n=j}^{q-1} l_n + e_{1,m}\right)}{e_{0,m} + \sum_{n}^{p} l_n + e_{1,m}} \tag{11}$$

where

$$p \le i \le j \le q$$

$$\sum_{n=p}^{i-1} l_n = 0 \ \text{ for } \ i = p$$

$$\sum_{n=j}^{q-1} l_n = 0 \ \text{ for } \ j = q$$

As U_m must satisfy Eq. (3) to be a local minimum, from Eqs. (7), (9), and (10), we obtain

$$K_{L,m} = K_{R,m} \quad (= K_m) \tag{12}$$

which indicates that both sides of the antagonistic muscles are driven by the same force simultaneously.

From Eqs. (8)–(12), the following equations are obtained:

$$H_{m,ij} = 2K_m \left\{ a_m^2 - \left(S_m - s_{0,m}\right) \frac{\left(e_{0,m} + \sum_{n=p}^{i-1} l_n\right)\left(\sum_{n=j}^{q-1} l_n + e_{1,m}\right)}{S_m} \right\}$$

$$= 2K_m \left\{ a_m^2 - \left(1 - \frac{s_{0,m}}{S_m}\right)\left(e_{0,m} + \sum_{n=p}^{i-1} l_n \right)\left(\sum_{n=j}^{q-1} l_n + e_{1,m} \right) \right\}$$

$$= 2K_m \left\{ a_m^2 - \varepsilon_{\mathrm{Max}}\left(e_{0,m} + \sum_{n=p}^{i-1} l_n \right)\left(\sum_{n=j}^{q-1} l_n + e_{1,m} \right) \right\} \tag{13}$$

$$H_{ij} = \sum_{m}^{M} 2K_m \left\{ a_m^2 - \varepsilon_{\mathrm{Max}}\left(e_{0,m} + \sum_{n=p}^{i-1} l_n \right)\left(\sum_{n=j}^{q-1} l_n + e_{1,m} \right) \right\} \tag{14}$$

where $\varepsilon_{\mathrm{Max}}$ is the maximum contraction ratio of the muscle, and the muscle length, S_m, can be obtained as

$$S_m = e_{0,m} + \sum_{n=p}^{q-1} l_n + e_{1,m}$$

We consider contraction ratio $\varepsilon_{\mathrm{Max}}$ to be always positive because the McKibben artificial muscles are assumed to be of contraction type. Therefore, the second term related to $\varepsilon_{\mathrm{Max}}$ in Eq. (14) is always negative. Thus, a larger a_m leads to more positive elements, H_{ij}, in the Hessian matrix, and larger $e_{0,m}$, $e_{1,m}$, and link lengths lead to more negative elements. From Eq. (14), we can anticipate the stability of the system by H_{ij} satisfying Eq. (4) or Eq. (5).

Stability of monoarticular and multiarticular muscles

If any diagonal element of the Hessian matrix of potential energy is negative, Eq. (4) cannot be satisfied because any negative H_{ii} results in the following left-hand side of Eq. (4) by setting $\boldsymbol{x}$ as $\boldsymbol{x} = (0..x_i..0)^T, x_i \in \boldsymbol{R}$:

$$\boldsymbol{x}^T \boldsymbol{H} \boldsymbol{x} = H_{ii} x_i^2 < 0$$

The condition above is related to the stability of joint i but not to that of the entire system. Therefore, for system stability, all the diagonal elements of the Hessian matrix should be positive.

When joints q and p are the same, that is, when considering antagonistic monoarticular muscles that span joint *p*, the corresponding Hessian matrix of potential energy is given by

$$H_{m,ij} = \begin{cases} 2K_m\{a_m^2 - \varepsilon_{Max} e_{0,m} e_{1,m}\} & (\text{if } i = j = p) \\ 0 & (\text{otherwise}) \end{cases} \quad (15)$$

Equation (15) shows that monoarticular muscles affect only the *p*-th diagonal element of the Hessian matrix, H_{pp}. As the diagonal elements must be positive for stability, the antagonistic pairs of monoarticular muscles stabilize joint *p* when $H_{m,pp}$ is positive, which can be expressed as follows:

$$a_m^2 - \varepsilon_{Max} e_{0,m} e_{1,m} > 0 \quad (16)$$

Equation (16) indicates that $e_{0,m}$ and/or $e_{1,m}$ must be sufficiently smaller than a_m for the monoarticular muscles to stabilize the joint.

When joints q and p are different, the diagonal elements of the Hessian matrix of potential energy produced by antagonistic multiarticular muscles can expressed as

$$H_{m,ii} = \begin{cases} 2K_m\left\{a_m^2 - \varepsilon_{Max}\left(e_{0,m} + \sum_{n=p}^{i-1} l_n\right)\left(\sum_{n=i}^{q-1} l_n + e_{1,m}\right)\right\} & (\text{if } p < i < q) \\ 2K_m\left\{a_m^2 - \varepsilon_{Max} e_{0,m}\left(\sum_{n=i}^{q-1} l_n + e_{1,m}\right)\right\} & (\text{if } i = p) \\ 2K_m\left\{a_m^2 - \varepsilon_{Max}\left(e_{0,m} + \sum_{n=p}^{i-1} l_n\right) e_{1,m}\right\} & (\text{if } j = q) \\ 0 \quad (\text{otherwise}) \end{cases} \tag{17}$$

In Eq. (17), the p-th and q-th diagonal elements become positive if $e_{0,m}$ and $e_{1,m}$ are sufficiently close to 0. In contrast, the diagonal elements for joints between p and q are usually negative because a_m is not much larger than the sum of the link lengths. Thus, multiarticulate antagonistic muscles cause instability, especially for the joints between them.

Results

Simulations

We first validated our formulation through calculations and simulations implemented in MathWorks MATLAB Simulink.

For the simulations and the experiments reported below, we considered a three-joint multi-serial-link mechanism with four pairs of antagonistic muscles comprising three pairs of monoarticular muscles and one pair of tri-articular muscles. The parameters of the McKibben artificial muscles are listed in Table 1 and were consistent for the simulations and experiments.

Table 1 Parameters of multi-serial-link mechanism

$\boldsymbol{l_0}$ [mm]	l_1 [mm]	l_2 [mm]	l_3 [mm]	a [mm]	h [mm]
50	50	50	50	19.5	9

In the experimental equipment, there were differences between the heights of both muscle endpoints. Therefore, we set the height gap to $h = 9$ mm. Moreover, the vertical distance of all muscles from links $a_1, \ldots, a_4$ was set to 19.5 mm. Figure 4 shows a diagram of the mechanism considering the parameters listed in Table 1. Assuming that the antagonistic artificial muscles are tilted by ψ in the height direction from the horizontal line, the default muscle length, S_m, and the vectors of the antagonistic muscles vary from those mentioned above. As a result, the Hessian matrix of the potential energy produced by the muscles derived from Eq. (13) can be rewritten as follows:

$$H_{m,ij} = 2K_m \left\{ (\cos^2\psi + \varepsilon \sin^2\psi) a_m^2 - \varepsilon_{\mathrm{Max}} \left(e_{0,m} + \sum_{n=p}^{i-1} l_n \right) \left(\sum_{n=j}^{q-1} l_n + e_{1,m} \right) \right\} \tag{18}$$

with angle ψ given by

$$\psi = \tan^{-1} \frac{h}{S_m}$$

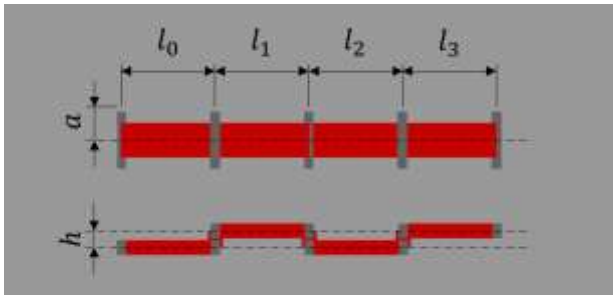

Fig. 4 Diagram of multi-serial-link mechanism

Table 2 lists the experimental parameters of the monoarticular and tri-articular muscles and of the McKibben artificial muscles. The stiffness of the artificial muscles, K_m, was derived from Eq. (2) for F_{Max} obtained using Eq. (1). In addition, $\varepsilon_{\mathrm{Max}}$ was determined from measurements on a tri-articular muscle at varying applied pressure P. Specifically, the monoarticular muscles and tri-articular muscles were driven by air pressures of 0.0, 0.3, 0.4, and 0.5 MPa. We measured 15 trials per air pressure except

for the pressure of 0.0 MPa, which is equivalent to the muscles being not attached to the joint because no interference occurs to the muscles and links in the simulation. The simulations results are shown in Fig. 5.

Table 2 Parameters of McKibben artificial muscles

Parameter	Monoarticular muscle			Tri-articular muscle		
P (MPa)	0.3	0.4	0.5	0.3	0.4	0.5
K_m (kN/m)	2.26	2.45	2.58	0.57	0.62	0.66
$\varepsilon_{\mathrm{Max}}$ (%)	13	16	19	13	16	19
e_0 (mm)		0			50	
e_1 (mm)		50			50	

Rubber tube outer diameter D = 2 mm

Rubber tube inner diameter d = 1.16 mm

Sleeve default angle θ_0 = 19°

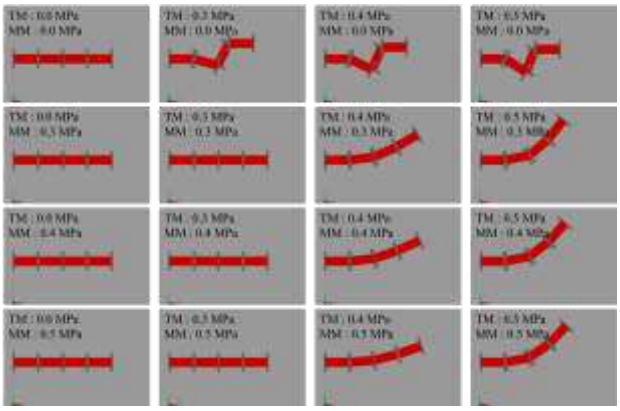

Fig. 5 Results of dynamic simulations. One spring that represents a tri-articular muscle (TM) is attached to both ends of the system, and three springs that represent monoarticular muscles (MMs) are attached around each joint

Using the values in Tables 1 and 2, the determinants of $\boldsymbol{A}_1$, $\boldsymbol{A}_2$, and $\boldsymbol{A}_3$ defined in Eq. (5) are obtained as listed in Table 3. When no pressure (0.0 MPa) is applied to the monoarticular muscles and when pressure of 0.4 or 0.5 MPa is applied to the tri-articular muscles, at least one of the determinants from $\boldsymbol{A}_1$, $\boldsymbol{A}_2$, and $\boldsymbol{A}_3$ becomes negative. Thus, instability occurs as confirmed by the simulation

results shown in Fig. 5. When the determinant of $\boldsymbol{A_1}$ is negative, instability appears as zigzag buckling.

Table 3 Determinants of $\boldsymbol{A_1}$, $\boldsymbol{A_2}$, and $\boldsymbol{A_3}$ indicating stability in different cases

		Air pressure of tri-articular muscles (MPa)			
		0.0	0.3	0.4	0.5
Air pressure of monoarticular muscles (MPa)	0.0	$\lvert\boldsymbol{A}_1\rvert = 0$	−0.68	−1.02	−1.37
		$\lvert\boldsymbol{A}_2\rvert = 0$	0.63	1.28	2.17
		$\lvert\boldsymbol{A}_3\rvert = 0$	−0.35	−1.04	−2.32
	0.3	1.68	0.99	0.65	0.31
		2.81	0.52	−0.17	−0.66
		4.70	0.42	−0.31	−0.51
	0.4	1.82	1.13	0.80	0.45
		3.30	0.76	−0.04	−0.64
		5.99	0.76	−0.26	−0.67
	0.5	1.91	1.23	0.89	0.54
		3.66	0.96	0.08	−0.60
		7.01	1.07	−0.19	−0.77

Experiments

We also verified our formulation experimentally using a three-joint multi-serial-link mechanism and McKibben artificial muscles. A diagram and photograph of the experimental system are shown in Fig. 6. The air pressure provided by an air compressor was adjusted using a pressure valve and applied to the monoarticular and tri-articular muscles. To reduce the effects of friction between the link and ground and in the joints, the weight of the links was reduced by fabricating them with a 3D printer, and bearings were used at each joint. The McKibben muscles used in the experiment had the parameters listed in Table 2.

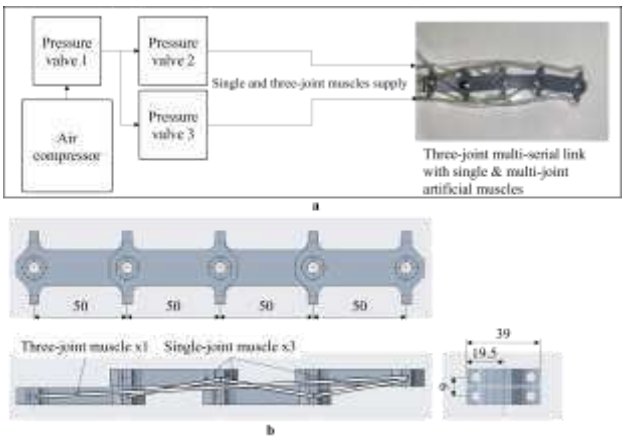

Fig. 6 a Diagram and photograph of experimental equipment and **b** diagram of multi-serial-link mechanism showing dimensions and attachment points of monoarticular and multiarticular muscles (unit: millimeters)

The same cases evaluated in the simulations were tested experimentally, obtaining the experimental results shown in Fig. 7. When the pressure applied to the monoarticular muscles is 0.0 MPa, each joint angle changes substantially, clearly destabilizing the system at the target posture. When monoarticular muscles are driven at any pressure except for 0.5 MPa and tri-articular muscles are driven at 0.4 or 0.5 MPa, the joint angles change in a smaller proportion than without using the monoarticular muscles. When the monoarticular muscles are driven at 0.5 MPa, it is difficult to recognize the changes. When the monoarticular muscles are driven at 0.3 MPa, no remarkable changes occur regardless of the pressure applied to the tri-articular muscles. Overall, the experimental results are consistent with those obtained from our formulation.

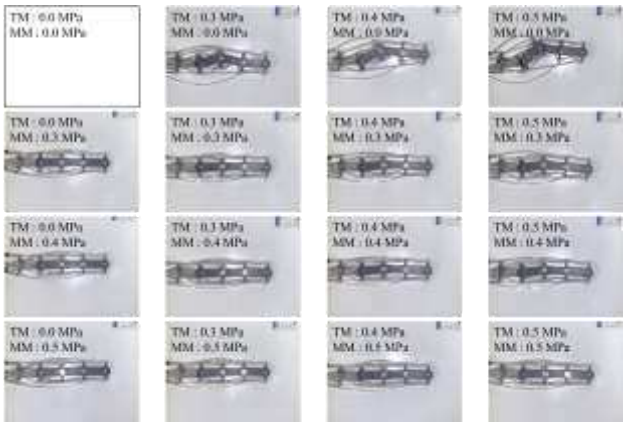

Fig. 7 Experimental results. Monoarticular and tri-articular muscles were actuated at air pressures of 0.0, 0.3, 0.4, and 0.5 MPa

Discussion

The results in Table 3 show that the system becomes theoretically unstable at target posture $\boldsymbol{\theta} = \mathbf{0}$ for monoarticular muscles driven at 0.0 MPa or tri-articular muscles driven at 0.4 or 0.5 MPa. In particular, when the monoarticular muscles are inactive (0.0 MPa), the determinant of $\boldsymbol{A}_1$ becomes negative, and the serial-link mechanism buckles in zigzag in both the simulation and experimental results (Figs. 5 and 7). In other theoretically unstable conditions, the simulation results in Fig. 5 show that the system bends like a bow. On the other hand, the experimental results shown in Fig. 7 show apparent instability of the serial-link mechanism because changes in each joint angle can be observed, but the mechanism does not bend with the extent shown in the simulations. In theoretically stable conditions, in which the tri-articular muscles are driven at 0.0 or 0.3 MPa, the mechanism does not bend and remains stable, as verified in the simulation and experimental results.

When the tri-articular muscles are driven at 0.5 MPa, the mechanism tends to stabilize as the

monoarticular muscles are driven at higher pressures in the experiments, contradicting the simulation results. This inconsistent result is attributable to the effect of joint friction, which increases with the muscle contraction forces.

In addition to the effect of joint friction, the friction caused by the interference between the artificial muscles and links tends to stabilize the posture of the mechanism. Therefore, the serial-link mechanism can remain stable at a posture around the target, at least when the theoretically stable conditions are satisfied.

Conclusion

Considering monoarticular and multiarticular muscles in a multiarticulate musculoskeletal system, we analyze the conditions for system stability while driving the multiarticular muscles. Theoretically, we determine stability assuming that it can be reached when the potential energy produced by each articular muscle is locally minimal at the target point. In addition, the distances from the fixed point of the monoarticular muscles to the joint, $e_{0,m}$ and $e_{1,m}$, must be sufficiently small to stabilize each joint. We analyzed the stability of a three-joint multiarticulate musculoskeletal system and validated our formulation through dynamic simulations and experiments on a mechanism driven by McKibben artificial muscles. We confirmed that a sufficiently high stiffness of monoarticular muscles and a locally minimal potential energy of the system at the target posture lead to stability in the musculoskeletal mechanism consisting of serial links and multiarticulate McKibben muscles.

Declarations

Acknowledgments

This work was supported by JSPS KAKENHI Grant-in-Aid for Scientific Research(A) under Grant Number JP18H03760.

We would like to thank Editage (www.editage.com) for English language editing.

Authors' contributions

YI carried out analysis and experiment and drafted the manuscript. HN, GE, and KS were involved to the study design and data interpretation. All authors revised the report, commented on the draft of the manuscript, and approved the final report.

Funding

This work was supported by the JSPS KAKENHI Grant-in-Aid for Scientific Research(A) under Grant Number JP18H03760.

Availability of data and materials

Not applicable.

Competing interests

The authors declare that they have no competing interest.

References

1. Niikura A, H Nabae, G Endo, M Gunji, K Mori, R Niiyama, K Suzumori (2020) Prototyping of

musculoskeletal robot based on anatomy of a giraffe neck and static analysis of longus colli muscle. Paper presented at the robotics and mechatronics conference 2020 in Kanazawa, 27-30 May 2020. (In Japanese).

2. Garriga-Casanovas A, Faudzi AM, Hiramitsu T, Rodriguez y Baena F, Suzumori K (2017) Multifilament pneumatic artificial muscles to mimic the human neck. In: Proceedings of the 2017 IEEE International Conference on Robotics and Biomimetics (ROBIO), Macau, Macao, pp. 809–816

3. Oh S, Hori Y (2009) Development of two-degree-of-freedom control for robot manipulator with biarticular muscle torque. In: 2009 American Control Conference, St. Louis, MO, pp. 325–330. doi: 10.1109/ACC.2009.5160742

4. Salvucci V, Kimura Y, Oh S, Koseki T, Hori Y (2013) Comparing approaches for actuator redundancy resolution in biarticularly-actuated robot arms. IEEE/ASME Trans Mechatron 19(2):765–776. doi: 10.1109/TMECH.2013.2257826

5. Ochi H, Kino H, Tahara K, Matsutani Y (2020) Geometric conditions of a two-link-and-six muscle structure based on internal force stability. ROBOMECH J 7(1):1–16. doi: 10.1186/s40648-020-00164-3

6. Ruppert F, Badri-Spröwitz A (2019) Series elastic behavior of biarticular muscle-tendon structure in a robotic leg. Front Neurorobot 13:64. doi: 10.3389/fnbot.2019.00064

7. Kaneko T, Sekiya M, Ogata K, Sakaino S, Tsuji T (2016) Force control of a jumping musculoskeletal robot with pneumatic artificial muscles. In: 2016 IEEE/RSJ International Conference on Intelligent Robots and Systems (IROS), Daejeon, Republic of Korea, pp. 5813–5818. doi: 10.1109/IROS.2016.7759855

8. Hosoda K, Sakaguchi Y, Takayama H, Takuma T (2010) Pneumatic-driven jumping robot with anthropomorphic muscular skeleton structure. Auton Robot 28(3):307–316. doi: 10.1007/s10514-009-9171-6

9. Mizuuchi I, Inaba M, Inoue H (2001) A flexible spine human-form robot-development and control of the posture of the spine. In: Proceedings of the 2001 IEEE/RSJ International Conference on Intelligent Robots and Systems, Maui, HI, pp. 2099–2104. doi: 10.1109/IROS.2001.976381

10. Mizuuchi I, Tajima R, Yoshikai T, Sato D, Nagashima K, Inaba M, Kuniyoshi Y, Inoue H (2002) The design and control of the flexible spine of a fully tendon-driven humanoid “Kenta”. In: IEEE/RSJ International Conference on Intelligent Robots and Systems, Lausanne, Switzerland, pp. 2527–2532. doi: 10.1109/IRDS.2002.1041649

11. Tsuji T (2010) A model of antagonistic triarticular muscle mechanism for lancelet robot. In: 2010 11th IEEE International Workshop on Advanced Motion Control, Nagaoka, Japan, pp. 496–501. doi: 10.1109/AMC.2010.5464082

12. Kano T, Sato T, Kobayashi R, Ishiguro A (2011) Decentralized control of multi-articular snake-

like robot for efficient locomotion. In: 2011 IEEE/RSJ International Conference on Intelligent Robots and Systems, San Francisco, CA, pp. 1875–1880. doi: 10.1109/IROS.2011.6094712

13. Astley HC (2020) The biomechanics of multi-articular muscle–tendon systems in snakes. Integr Comp Biol 60(1):140–155. doi: 10.1093/icb/icaa012

14. Ozawa R, Kobayashi H (2001) Set-point Force Control of Tendon-driven Robotic Mechanisms with Nonlinear Tendon Elasticity. Journal of the Robotics Society of Japan, 19(3):372–379. (In Japanese)

15. Schulte HF (1961) The characteristics of the McKibben artificial muscle. Appl Extern Power Prosthet Orthot 94–115